D. Fritsch, M. Englich & M. Sester, eds, 'IAPRS', Vol. 32/4, ISPRS Commission IV Symposium on GIS - Between Visions and Applications, Stuttgart, Germany.

MOSAICKING OF DIGITAL ELEVATION MODELS DERIVED BY SAR INTERFEROMETRY

Walter Knöpfle, Günter Strunz, Achim Roth
German Remote Sensing Data Center
German Aerospace Center, DLR
Oberpfaffenhofen
D-82234 Wessling, Germany
email: {Walter.Knoepfle | Guenter.Strunz | Achim.Roth}@dlr.de
phone: +49 8153 28 1384
fax: + 49 8153 28 1445

ABSTRACT

In the framework of the Shuttle Radar Topography Mapper (SRTM) Mission the generation of high-quality Digital Elevation Models (DEMs) with global coverage of the earth's surface is envisaged. In this mission, which is scheduled for late 1999 on NASA's space shuttle, single-pass Interferometric Synthetic Aperture Radar (InSAR) data will be acquired and processed. The German Aerospace Center DLR will process, archive and distribute the data delivered by the X-band system X-SAR. In preparation for this mission DLR's Remote Sensing Data Center (DFD) is implementing an InSAR processing chain for the derivation of DEMs, which provides operational product generation as well as multi-mission capabilities. This comprises subsystems for screening and transcription, the interferometric SAR processing, the geocoding and mosaicking, and the database system for efficient handling and archiving of multi-resolution DEMs.

The paper at hand describes the generation of DEM mosaics from different sources, primarily based on interferometric SAR. The main parameters, which influence the accuracy of the height determination, are briefly discussed and the concept of height error maps, representing the accuracy of the corresponding DEMs, is outlined. The mosaicking of the DEMs resulting from various sources, mainly ERS tandem data from ascending and descending orbits, is described. The mosaicking takes into account the different prior accuracy of the DEMs and derives the quality of the resulting DEM. The method is illustrated by practical examples and an outlook is given on further investigations.

1 INTRODUCTION

Interferometric Synthetic Aperture Radar (InSAR) is a rapidly developing technology for the generation of Digital Elevation Models (DEMs). Although the basic principle dates back to the early 70's (Graham, 1974), the use of spaceborne InSAR has only been intensively investigated after the launch of ERS-1 (e.g. Prati, Rocca, 1993, Massonnet, Rabaute, 1993, Hartl et al., 1994, Zebker et al., 1994).

With ERS-1/2 tandem data, *repeat-pass* interferometry with a one day difference between both acquisitions became feasible. *Single-pass* interferometry is envisaged in the planned Shuttle Radar Topography Mapper (SRTM) Mission, which is scheduled for late 1999. This mission is the third flight of the Shuttle Radar Laboratory, a joint project of the USA, Italy and Germany. It is modified to enable single-pass interferometry by adding a second passive antenna mounted on a 60 m boom. Within the geographical latitude of +/-60 degrees high-quality digital elevation models with global coverage of the earth's surface (80% of the land mass) will be generated.

DLR's Remote Sensing Data Center (DFD) is implementing an InSAR processing chain for the derivation of DEMs, which provides product generation on an operational basis as well as multi-mission capabilities. This comprises software for the interferometric SAR processing, the geocoding and mosaicking of DEMs, and the database system for efficient handling and archiving of multi-resolution DEMs.

The paper describes recent developments at DFD concerning the mosaicking of digital elevation models resulting from different sources. These procedures aim at the automatic generation of DEM mosaics based on interferometric SAR from the SRTM mission as well as repeat-pass InSAR from ERS-Tandem data. In principle, existing global DEMs resulting from databases like GLOBE or local DEMs from digitized contour maps or optical stereo data can be incorporated in the mosaicking, as well.

The concept for the generation of digital elevation models by InSAR methods is briefly described. The main parameters, which influence the accuracy of the height determination, are discussed for the single-pass as well as for the repeat-pass interferometry. Furthermore, the concept of height error maps, describing the accuracy of the corresponding DEMs, is outlined. The mosaicking of the DEMs resulting from various sources, mainly ERS-tandem data from ascending and descending orbits, is explained. It takes into account the different prior accuracies of the DEMs, which are represented in the corresponding height error maps. Furthermore, statistical outlier tests are incorporated in the procedure, in order to eliminate possible gross errors in the input data. For the resulting DEM mosaic also a corresponding height error map is calculated by error propagation, which is stored in the DEM data base. Some practical examples are shown, which illustrate the realization of the concept. Finally, an outlook is given on further investigations.

D. Fritsch, M. Englich & M. Sester, eds, 'IAPRS', Vol. 32/4, ISPRS Commission IV Symposium on GIS - Between Visions and Applications, Stuttgart, Germany.

2 DEM GENERATION

2.1 Interferometric SAR

SAR interferometry exploits the phase of SAR signals to measure differences to an accuracy of a fraction of the wavelength. Phase differences of two complex-valued SAR images of the same area, but from slightly different orbits, are computed on a pixel-by-pixel basis (Bamler, 1997). A detailed description can be found e.g. in Schwäbisch (1995). Figure 1 shows the principle of repeat-pass and single-pass interferometry.

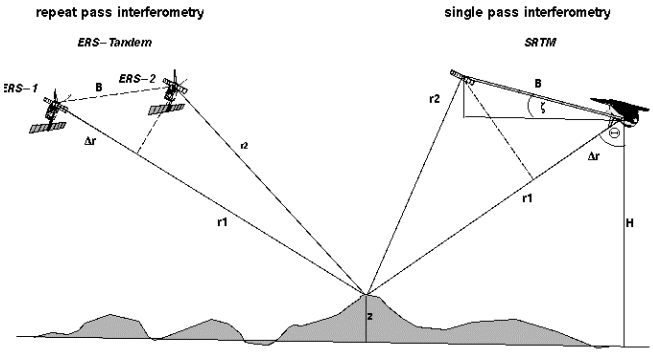

Figure 1: Repeat- and single-pass interferometric SAR

2.2 Production chain

The entire processing chain comprises four subsystems, the screening and transcription sytem, the SAR processor, the generic system for interferometric SAR, and the geocoding and mosaicking system. Within DFD's InSAR production system the interferometric processing comprises spectral shift filtering, slope adaptive filtering, coregistration, multilooking, coherence estimation, flat earth phase removal, and several phase unwrapping procedures (Eineder, Adam, 1997).

The geocoding and mosaicking system derives the DEM from the unwrapped phase image. The absolute phase is converted into height values and the slant range heights are geocoded into the DEM. The product quality is improved by the use of ground control points. This adjustment requires two different kinds of control points, i.e. for the correction of the timing parameters and for phase offset determination. Individual DEMs can be assembled to a DEM mosaic. Additionally, the system also produces data sets, which are suitable for other applications, as coherence maps, interferograms and amplitude images (Roth et al., 1998).

The final DEM product will be delivered to the user in tiles of 15 arc minutes extension in both latitude and longitude. A co-registered height error map will be provided as well, which describes the product quality.

3 DEM ACCURACY

3.1 Definition

The accuracy of DEMs is defined by the vertical and horizontal errors. The horizontal error is given as the difference between the measured and true location on ground; the vertical (height) error is defined as the difference between the measured height and the true height normal to the reference ellipsoid.

Height errors are given as absolute and relative values. The absolute accuracy is the standard deviation of the vertical error over all positions within a given area, the relative accuracy is the standard deviation of the high frequency component of the absolute error.

The performance requirements for SRTM aim at an absolute (relative) height error of 16 m (6 m) for 90% of the data, which is equivalent to a standard deviation of about 10 m (4 m). For ERS-1/2 tandem data the goal is to achieve an absolute height error of 30 m for 90% of the data (standard deviation ~18 m) to meet the DTED2 standard.

3.2 Height error sources

The accuracy of an interferometrically generated DEM is determined by 3 groups of error sources (Bamler, 1997):

- Phase noise: measurement accuracy of the phase
- Imaging geometry: accuracy of the orbit
- Atmospheric distortions: wave propagation conditions

3.2.1 Phase accuracy

The random phase error (phase noise) $\sigma\phi$ results in a height error of

$$\sigma z_{\Phi} = \frac{\lambda r \sin\theta}{2k\pi B\cos(\theta-\zeta)}\sigma\Phi$$

where λ is the wavelength, r is the slant range distance, θ is the look angle, ζ is the baseline tilt angle and B is the absolute baseline length as given in Figure 1 (k = 1 for single-pass and k = 2 for repeat-pass interferometry).

Phase noise originates from different sources, mainly from system noise (receiver and quantization noise) and temporal scene decorrelation in case of repeat-pass interferometry. The standard deviation of the phase can be estimated as a function of coherence and number of looks (Just, Bamler, 1994, Bamler, Hartl, 1998), where the coherence is defined as the mutual correlation coefficient between the two images. This dependency is illustrated for 5 looks in Figure 2.

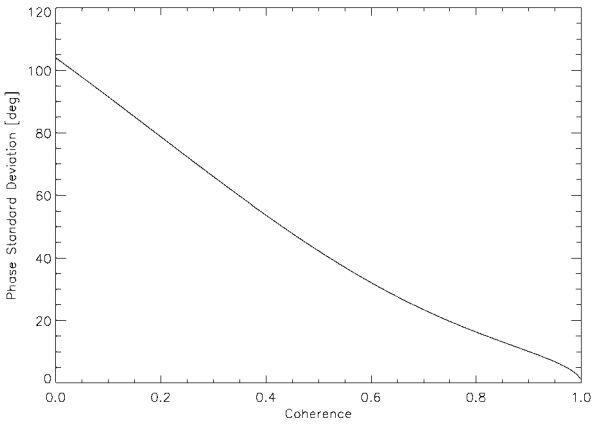

Figure 2: Standard deviation of the phase as a function of coherence (number of looks: 5)

D. Fritsch, M. Englich & M. Sester, eds, 'IAPRS', Vol. 32/4, ISPRS Commission IV Symposium on GIS - Between Visions and Applications, Stuttgart, Germany.

3.2.2 Imaging geometry

The errors resulting from the imaging geometry can be mainly described by the following sources (Rodriguez, Martin,1992):

- Baseline length error σB
- Baseline tilt angle error $\sigma\zeta$
- Slant range error σr
- Altitude error σH
- Position error σx

The influence of these errors on the resulting height error can be derived by differentiating the basic interferometric equations. According to Rodriguez, Martin (1992) this results in the following equations:

$$\sigma z_B = \frac{r \tan(\theta - \zeta) \sin\theta}{B} \sigma B$$

$$\sigma z_\zeta = r \sin\theta \sigma\zeta$$

$$\sigma z_r = \cos\theta \sigma r$$

$$\sigma z_H = \sigma H$$

$$\sigma z_x = \sin\theta \sigma x$$

Additionally, an overall system error including calibration errors can be taken into account.

3.2.3 Atmospheric distortions

For repeat-pass interferometry several phenomena due to different wave propagation conditions can appear. Tropospheric water vapour may cause phase shifts in the interferograms, which lead to cloud-like or ripple-like phase structures. In practice, these are difficult to model, therefore, they have to be eliminated e.g. by using several interferograms for the DEM generation.

3.2.4 Resulting height error

The total height error is the root sum square of all independent height error contributions:

$$\sigma z_{total} = \sqrt{\sigma z_\Phi{}^2 + \sigma z_B{}^2 + \sigma z_\zeta{}^2 + \sigma z_r{}^2 + \sigma z_H{}^2 + \sigma z_x{}^2}$$

$$\sigma z_{total} = \sqrt{\sigma z_{phase}{}^2 + \sigma z_{geometry}{}^2}$$

3.3 Error budget for SRTM and ERS tandem

The actual error budgets depend on the mission parameters. For SRTM and ERS tandem mission the following parameter values are assumed:

	SRTM	ERS tandem
Wave length:	3.1 cm	5.7 cm
Slant range:	341 km	847 km
Look angle:	52 deg	23 deg
Baseline length:	62 m	variable
Baseline tilt angle:	45 deg	variable
Phase difference:	1580 deg	variable
With errors (standard deviation) in		
Slant range:	1.2 m	9 m
Baseline length:	2.4 mm	20 cm
Baseline angle:	5.5”	variable
Phase difference:	3 deg	20-40 deg

In case of SRTM the following height errors can be estimated based on the assumptions above. The main influence factors, i.e. the height error due to random phase error, the height error due to baseline length error, the height error due to baseline tilt angle error, and a height error due to an overall system error result in a total height error of about 9 m (~ 15 m for 90 % accuracy).

In case of ERS tandem the configuration of ERS-1 and ERS-2 is not fixed. Baseline lengths and tilt angles are variable and have to be derived from the orbits. The ERS orbits are only known with an accuracy of about +/-20 cm, which is an order of magnitude worse than with SRTM, where the baseline is directly observed. This requires an additional control point measurement and adjustment. Furthermore, the one day repeat pass configuration leads to decorrelation and occasionally to atmospheric distortions.

The height errors due to random phase errors for ERS tandem are given in Figure 3 for two different baseline lengths.

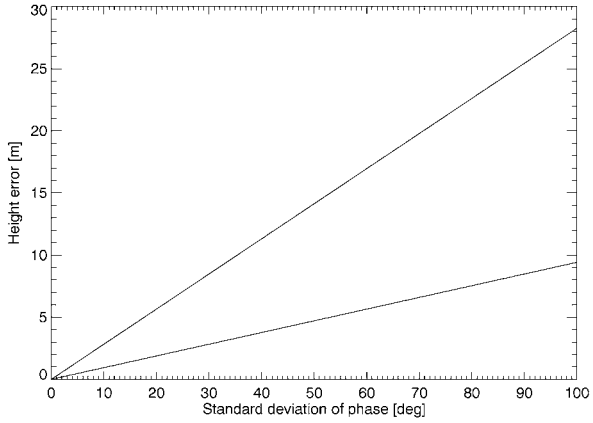

Figure 3: Height error due to phase noise
(for baseline length of 100 m (upper line) and of 300 m (lower line) and for baseline tilt angle of 45 deg)

The height errors due to errors in baseline length are given in Figure 4.

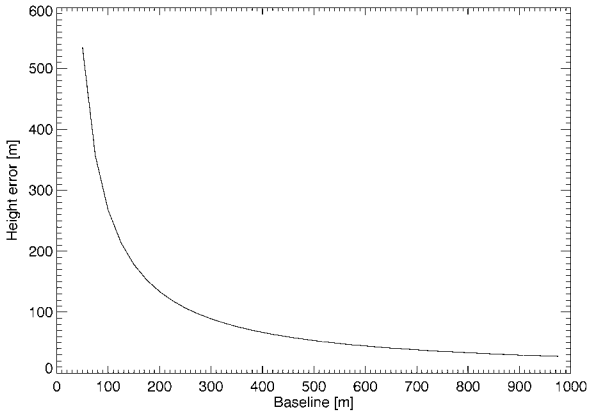

Figure 4: Height error due to baseline length error of 20 cm (for baseline tilt angle of 45 deg and different baseline lengths)

The height errors due to errors in baseline tilt angle are given in Figure 5. This error depends on uncertainties of orbit positions σp and baseline length B according to:

$$\sigma\zeta = \arctan(\frac{\sigma p}{B})$$

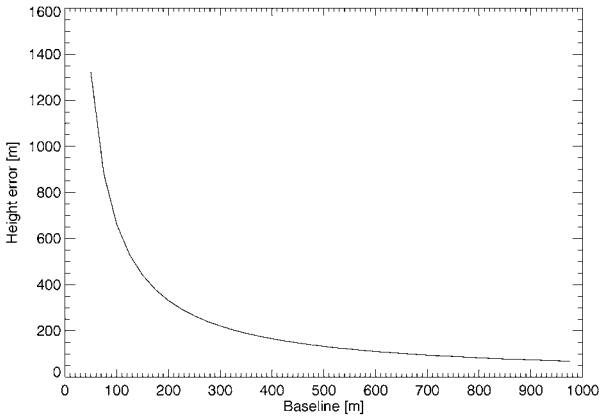

Figure 5: Height error due to baseline tilt angle error (for σp equal to 20 cm and different baseline lengths)

Figures 4 and 5 show that for ERS tandem data considerable height errors are to be expected. Therefore, substantial improvements over the initial geometry are necessary to meet the DTED2 height error requirements. This improvement can be achieved by the use of ground control points.

3.4 Improvement by control points

Whereas the height errors σz_{phase} resulting from the phase noise are of random nature, the height errors $\sigma z_{geometry}$ are due to the geometric configuration and its uncertainty. This initial geometry can be improved by a proper set of ground control points (GCPs). Then the errors $\sigma z_{geometry}$ can be partly improved by an error estimation based on control points.

Precondition is a well defined set of control points regularly distributed over the area of interest. Two types of control points are to be distinguished: Points with well defined location for the adjustment of the timing parameters, to minimize the horizontal location errors and points with well defined heights for the adjustment of the absolute phase, to minimize the vertical height errors.

This is achieved by a least square fit: a linear approach proved to be sufficient for the timing parameters, whereas for phase offset adjustment a two dimensional second order approach is required. This is equivalent to an improvement of the slave orbit and requires at least 6 phase control points. The standard deviation of the residuals of the used phase control points with respect to the corrected absolute phase can be used to define the remaining height error after the adjustment. This height error is usually smaller than the errors $\sigma z_{geometry}$ in case of ERS tandem.

To take into account the number of GCPs used, the statistical error bound for the standard deviation is calculated based on the χ^2-function. It includes the degrees of freedom in the least square fit with n control points and $u = 6$ unknown parameters. This is illustrated in Figure 6 for a height error of 20 m.

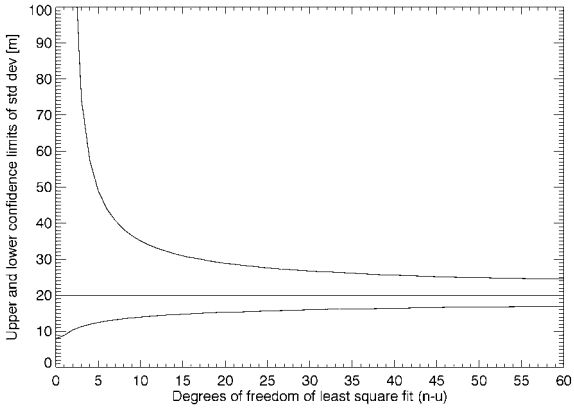

Figure 6: Upper and lower limit of standard deviation (for standard deviation of 20 m)

The upper limit of standard deviation σz_{GCP} is compared to the calculated $\sigma z_{geometry}$. If the accuracy based on the GCPs is better than $\sigma z_{geometry}$, which is in most cases true for ERS tandem, then it is replaced by σz_{GCP}. If not, then $\sigma z_{geometry}$ is used. The resulting total height error is then calculated according to:

$$\sigma z_{total} = \sqrt{\sigma z_{phase}^{\ 2} + \sigma z_{geometry/GCP}^{\ 2}}$$

3.5 Data border handling

Especially for the mosaicking of various DEMs (section 4) an additional border handling is included in the calculation of the accuracy. Towards the border of the DEM data there is an increasing uncertainty of the height values. This is mainly due to the processing with several filtering and resampling steps which negatively effects the data borders.

An additional feathering is recommended to take this into account. A moving window of 101 square pixels is used for weighting. The local weight is given by:

D. Fritsch, M. Englich & M. Sester, eds, 'IAPRS', Vol. 32/4, ISPRS Commission IV Symposium on GIS - Between Visions and Applications, Stuttgart, Germany.

$$p = \left((n - \frac{s^2}{2}) / (\frac{s^2}{2}) \right)^2$$

where *p* is the local weight, *n* is the coverage with valid height data and *s* is the size of the moving window. The weight *p* is equal to 1 inside the data and decreases to zero at the edges. The corresponding height error is then given by:

$$\sigma z_{Border} = \sqrt{1/p}$$

which is shown in Figure 7.

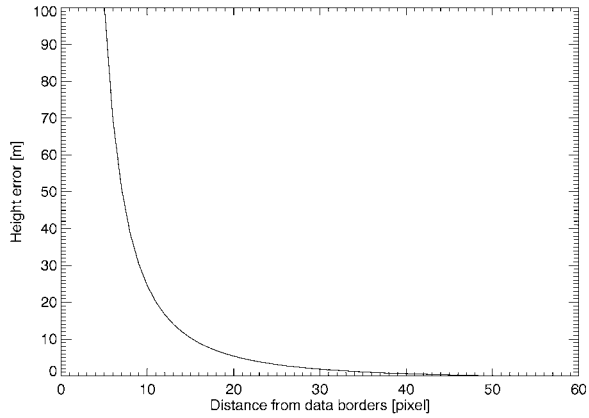

Figure 7: Additional height error due to data border handling

In case the border feathering is included, this results in a total height error of:

$$\sigma z_{total} = \sqrt{\sigma z_{phase}^2 + \sigma z_{geometry/GCP}^2 + \sigma z_{border}^2}$$

3.6 Height errors of DEMs from optical stereo data

As for the mosaicking, DEMs from various sources are used, the height errors of DEMs derived from optical stereo scanner data also have to be modeled. This is briefly described in the following. Similar to InSAR derived DEMs the error sources can be grouped into:

- Measurement noise: accuracy of point determination
- Imaging geometry: accuracy of exterior orientation

The measurement accuracy of each individual point can be derived from the matching procedure. If e.g. least squares matching is used, then the standard deviation of point determination can be estimated (Ackermann, 1984). This accuracy is mainly depending on the grey value gradients and the degree of correspondence of the homologous points in the matching procedure. An additional factor is the location of the points in the two images, which influences the geometric accuracy of the object point determination.

The accuracy resulting from the imaging geometry can be determined based on the inverse of the normal equation matrix of the least squares estimation of the exterior orientation parameters of the stereo images. The number and the definition of the orientation parameters depends on the mathematical model used for the line scanner imagery. The main influence parameters are the baseline length and height of the sensor platforms.

The resulting height error can be mainly described by:

$$\sigma z_{total} = \sqrt{\sigma z_{point(local)}^2 + \sigma z_{geometry(global)}^2}$$

3.7 Height error map

The height error is calculated for every pixel location within the DEM and the corresponding height error map is created. It represents the height error for every pixel within the data set and is used as input for the mosaicking.

4 DEM MOSAICKING

The mosaicking procedure creates large area DEMs from various input DEMs of the same coordinate system, along with the co-registered corresponding height error maps. Mosaicking of DEMs also includes compositing of DEM data sets for the same area. This is done by averaging the available height values within overlap areas. Proper weighting of the individual input height values is essential for this procedure.

The resulting height value is calculated according to:

$$z = \frac{1}{\sum_{i=1}^{n} p_i} (\sum_{i=1}^{n} z_i p_i); \qquad p_i = (\frac{1}{\sigma_i})^2$$

where *n* is the number of height values, z_i are the input height values and p_i are the weighting factors as given by the standard deviation σ_i of the input height error maps.

The resulting height value is estimated according to the least squares principle, which additionally provides the accuracy of the resulting height as:

$$\sigma_z = \sigma_0 \sqrt{\frac{1}{\sum p_i}}; \qquad \sigma_0^2 = \frac{\sum v_i^2 p_i}{n-1}$$

where σ_0 is the estimated variance factor and v_i are the residuals.

The detection of gross errors in the input heights is also included in the procedure. The outlier test investigates the hypothesis

$$H_0: \quad \max(abs(\frac{v_i}{\sigma v_i})) \le t_{n-u,\omega}$$

where v_i and σ_{vi} are the estimates for residuals and their standard deviations and *t* is the Student function with the degree of freedom (*n-u*) and the error probability ω.

The outlier test is being performed iteratively, and identified faulty values are excluded from averaging. This allows for a robust estimation of the resulting heights. The quality of the resulting DEM is thus determined by error propagation of the a priori accuracy as given by the corresponding input height error maps.

5 PRACTICAL EXAMPLE

5.1 Test Data

An area south west of Hannover was selected as test site. The area shows flat and hilly regions mainly covered with grassland and forests. Seven ERS-1/2 tandem data pair sets (two ascending and five descending orbit) were processed. The relevant parameters describing the data are listed in Table 1. Additionally a stereo pair from SPOT XS was included in the investigations.

DEM	Orbits	Frame	Quad.	Acquisition Date
1	20233/0649	2547	1	04/05-06-95
2	22326/2653	2547	1	22/23-10-95
3	23328/3655	2547	1	30/31-12-95
4	24831/5158	2547	1	14/15-04-96
5	24938/5265	1035	1	21/22-04-96
6	24938/5265	1053	4	21/22-04-96
7	25833/6160	2547	1	23/24-06-96
8	50	244		01/02-04-90

Table 1: Data sets used in the test site

Table 2 shows the values for baseline lengths and baseline tilt angles as well as the number of ground control points, which were measured in the data sets.

DEM	Baseline length	Baseline tilt angle	Number of time control points	Number of phase contr. Points
1	117 m	49 deg	47	48
2	108 m	0 deg	42	50
3	193 m	43 deg	38	46
4	93 m	44 deg	44	51
5	98 m	-2 deg	18	31
6	97 m	0 deg	48	31
7	110 m	48 deg	42	46
8	508 km	--	--	--

Table 2: Baseline parameters and number of measured control points

The standard deviations of the time control points resulted in less than 30 m horizontal error. This is an important precondition for the compositing of heights within the overlap areas. The resulting standard deviations of phase control points show height errors of 4 - 7 m. For the DEM from the SPOT stereo pair a set of 12 control points was measured resulting in a height standard deviation of 15 m.

5.2 DEM generation

In Figure 8 the input DEMs are shown as colour shaded relief representations.

The DEMs created from ERS-1/2 tandem pair data show very detailed topographic structures. However, small to medium atmospheric disturbances or low coherence lead to errors in the data. For instance, there are wave-like structures in DEM 2 (upper right) of magnitude of up to 20 m or cloud-like bubbles in DEM 4 (second row right). Low coherence in the DEMs 1 (upper left) and 7 (lower left) results in quite noisy height models, and missing fringes due to bad coherence lead to erroneous flat hill tops. The DEM 8 derived from the SPOT stereo pair (lower right) shows less detailed structures as compared to the InSAR DEMs.

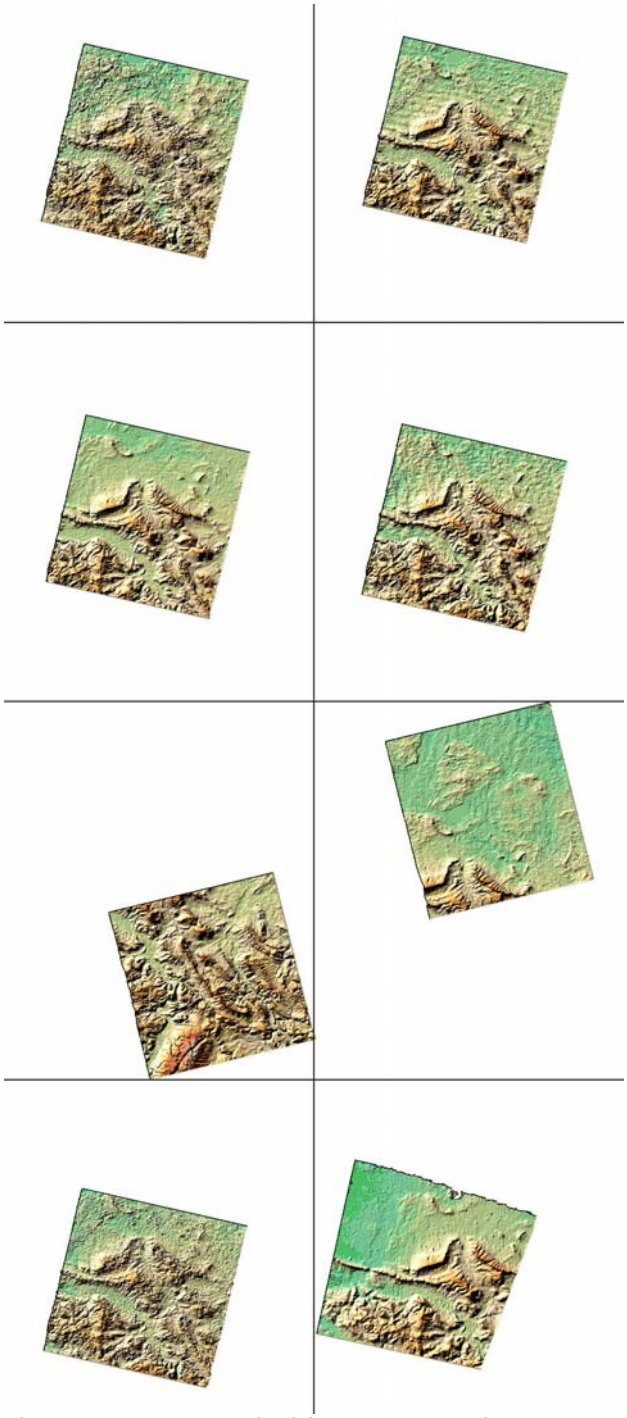

Figure 8: DEMs as result of the DEM generation

The accuracy of the individual eight DEMs was derived based on the described concept. Figure 9 shows an example of a height error map. The mean height error is about 15 m. Values from 7 to 15 m for grassland (dark values) and 12 to 22 m for forest regions (bright values) are mainly due to the differences in coherence.

D. Fritsch, M. Englich & M. Sester, eds, 'IAPRS', Vol. 32/4, ISPRS Commission IV Symposium on GIS - Between Visions and Applications, Stuttgart, Germany.

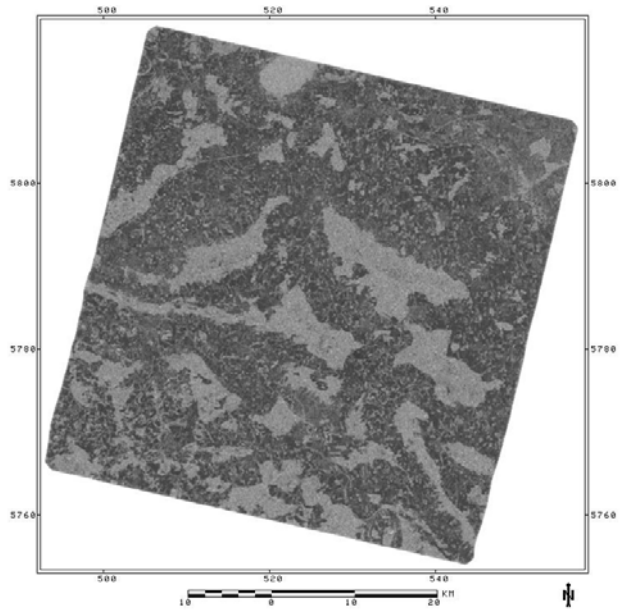

Figure 9: Height error map of DEM 2

In Table 3 an example is given, how the different parameters contribute to the total height error for a representative location within the data sets.

DEM	Local co-herence	Std dev of phase σ_ϕ	Height Error ΣZ_{phase}	Height Error σZ_{GCP}	Height Error σZ_{total}
1	0.488	55 deg	13.8 m	6.6 m	15.3 m
2	0.570	47 deg	12.4 m	6.8 m	14.1 m
3	0.539	50 deg	7.2 m	7.3 m	10.3 m
4	0.625	42 deg	12.6 m	5.7 m	13.8 m
5	0.133	91 deg	26.7 m	9.4 m	28.3 m
6	0.531	51 deg	14.9 m	6.5 m	16.3 m
7	0.535	50 deg	13.2 m	6.6 m	14.8 m
8	--	--	--	--	18.9 m

Table 3: Example for derivation of the total height error for a single location

5.3 Mosaicking

The mosaicking was done with the 8 input data sets taking into account the corresponding height error maps and including the outlier test. The result is shown in Figure 10.

Together with the mosaic, the resulting height error map and a coverage map are derived, which shows the number of used height values after the outlier test. For some hilly areas the number of input heights is reduced from initially 7-8 to 3-4 remaining values.

5.4 Quality assessment of the mosaicking concept

In order to evaluate the quality of the mosaicking procedure, a reference model is used. The DHM M745, provided by the German military mapping agency AmilGeo, is used for this purpose. Figure 11 shows this reference model, which covers an area of about 100 * 120 km.

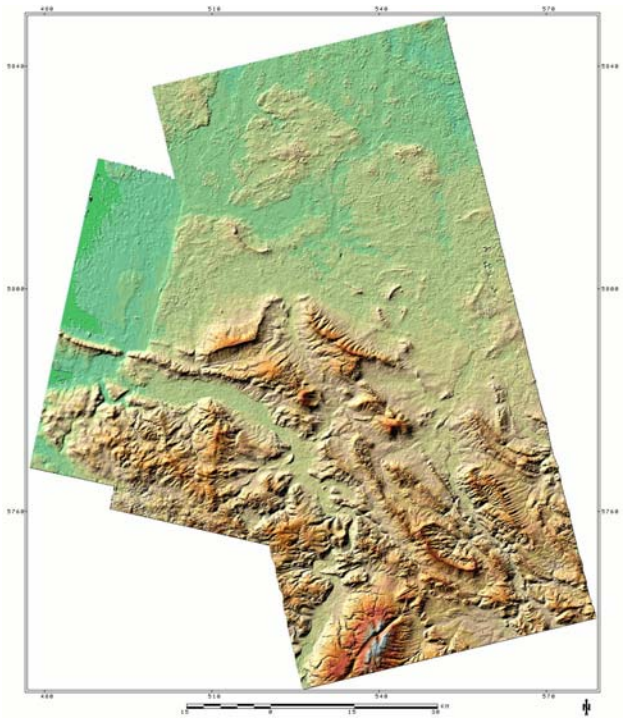

Figure 10: Mosaicking result from ERS-1/2 tandem data and SPOT stereo data

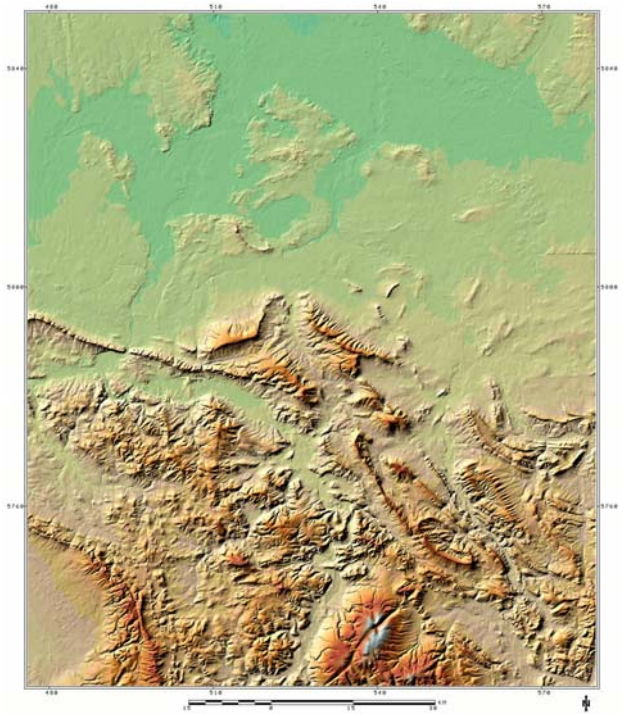

Figure 11: Reference model DHM M745 for the test site

The differences between the individual eight DEMs and the reference model are calculated in terms of root mean square (rms) errors. They resulted in errors from 12 m to 36 m, which fit quite well to the theoretical values derived by the concept of the height error maps.

For a detailed discussion a small part of the mosaic is investigated (15 * 17 km), a hilly region completely covered by forest, which is shown in Figure 12.

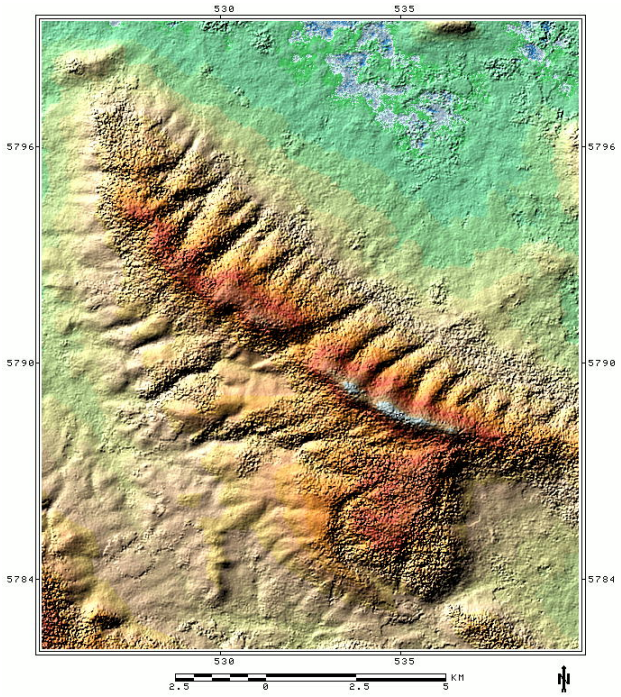

Figure 12: Detail area of the DEM mosaic

Three different mosaicking approaches are applied:

M1) Simple averaging of heights
M2) Weighted averaging of heights
M3) Weighted averaging of heights including outlier test

and the resulting DEM mosaic as well as the input DEMs are compared to the reference DHM M745. Table 4 shows the results of this evaluation.

DEM / Mosaicking approach	RMS errors	Height difference Percentage within +/-		
		8 m	16 m	32 m
1	55.1 m	37%	53%	74%
2	19.6 m	57%	81%	93%
3	15.8 m	80%	90%	94%
4	14.6 m	46%	79%	97%
5	16.5 m	60%	82%	94%
6	15.2 m	43%	70%	98%
7	48.8 m	43%	66%	79%
8	23.2 m	40%	62%	84%
M1	14.5 m	73%	85%	93%
M2	10.9 m	79%	90%	98%
M3	10.7 m	81%	95%	99%

Table 4: Evaluation results for the mosaicking approaches

In Table 4 the improvement by the mosaicking is visible. The rms errors of the mosaics are, except of method M1, considerably better than those of the individual input DEMs. Comparing the different mosaicking approaches, it can be seen, that M3 gives the best results.

Further improvements of the mosaicking procedure are under discussion. Concerning the height error estimation from phase control points, the simple global value will be replaced by a two-dimensional error function resulting from the least square fit. This will also take into account the distribution of the points. Another modification is the use of context-based instead of pixel-based averaging.

6 CONCLUSIONS

Recent developments at DFD concerning the mosaicking of digital elevation models resulting from different sources have been described. The results show, that the mosaicking considerably improves the quality of the DEM product. Further modifications of the algorithm will be performed and tested. The aim is to establish an operational system for the automatic generation of DEM mosaics based on interferometric SAR from the SRTM mission as well as repeat-pass InSAR from ERS-tandem data and also from DEMs, which result from existing databases, digitized contour maps or optical stereo data.

REFERENCES

Ackermann, F. (1984): Digital image correlation: performance and potential application in photogrammetry. Photogrammetric Record, 64(11), 429-439.

Bamler, R. (1997): Digital Terrain Models from Radar Interferometry. In: Fritsch, D., Hobbie, D. (Eds.): Photogrammetric Week ’97, Wichmann, Heidelberg, 93-105.

Bamler, R., Hartl, P. (1998): Synthetic Aperture Radar Interferometry. Review article submitted to *Inverse Problems.*

Eineder, M., Adam, N. (1997): A flexible system for the generation of interferometric SAR products. Proceedings IGARSS’97, Singapore.

Graham, L. C. (1974): Synthetic interferometer radar for topographic mapping. Proceedings IEEE, 63(6), 763-768.

Hartl, P., Thiel, K.-H., Wu, X., (1994): Information extraction from ERS-1 SAR data by means of InSAR and D-InSAR techniques in antarctic research. Proceedings 2nd ERS-1 Symposium, Hamburg, 697-701.

Just, D., Bamler, R. (1994): Phase statistics of interferograms with applications to synthetic aperture radar. Applied Optics, 33(20), 4361-4368.

Massonnet, D., Rabaute, T. (1993): Radar interferometry: limits and potential. IEEE Transactions on Geoscience and Remote Sensing, 31(2), 455-464.

Prati, C., Rocca, F. (1993): Improving slant range resolution with multiple SAR surveys. IEEE Transactions on Aerospace and Electronic Systems, 29(1), 135-144.

Rodriguez, E., Martin, J.M. (1992): Theory and Design of Interferometric Synthetic Aperture Radars. IEEE Proceedings-F, 139(2), 147-159.

Roth, A., Knöpfle, W., Hubig, M., Adam, N. (1998): Operational Interferometric SAR Products. Proceedings IGARSS’98, Seattle.

Schwäbisch, M. (1995): Die SAR-Interferometrie zur Erzeugung digitaler Geländemodelle. DLR-Forschungsbericht 95-25.

Zebker, H. A., Werner, C. L., Rosen, P. A., Hensley, S. (1994): Accuracy of topographic maps derived from ERS-1 interferometric radar. IEEE Transactions on Geoscience and Remote Sensing, 32(4), 823-836.